

The background is a solid purple color with several abstract geometric elements. A large, semi-transparent circular graphic is centered on the right side, featuring concentric rings and a dotted border. Diagonal lines and a grid of small dots are also visible, creating a sense of depth and movement.

III-5

Life, Earth and
Planetary Sciences

BL1U

Optical Activity Emergence in Amino-Acid Films by Vacuum-Ultraviolet Circularly-Polarized Light Irradiation (III) - Summary of Experiments -

J. Takahashi¹, T. Sakamoto¹, Y. Izumi², K. Matsuo², M. Fujimoto³, M. Katoh^{2,3},
Y. Kebukawa¹ and K. Kobayashi¹

¹Faculty of Engineering, Yokohama National University, Yokohama 250-8501, Japan

²Hiroshima Synchrotron Radiation Center, Higashi-Hiroshima 739-0046, Japan

³UVSOR Synchrotron Facility, Institute for Molecular Science, Okazaki 444-8585, Japan

One of the most attractive hypotheses for the origin of homochirality in terrestrial biomolecules (L-amino acid and D-sugar dominant) in the context of astrobiology is “Cosmic Scenario” [1,2]. Several ground experiments to validate the scenario have been investigated using circularly polarized light (CPL) from high-energy particle accelerators. We have already reported optical activity emergence in solid films of racemic amino acids by CPL irradiation of 215 nm in wavelength from free electron laser (FEL) of UVSOR-II [3].

Circular dichroism (CD) spectroscopy can detect optical activity emergence with a high accuracy because CD spectra sensitively reflects the steric structures of chiral molecules. The theoretical calculation of CD spectrum of L-alanine molecule has revealed that the absorption bands of carboxyl and amino groups are derived from electronic transitions ($n-\pi^*$, $\pi-\pi^*$, $n-\sigma^*$) corresponding to wavelengths below 230 nm (Fig.1) [4]. It is suggested that optical activity emergence by asymmetric photochemical reactions depends on the photon energy of CPL.

We carried out irradiation experiments by using CPL with different wavelengths to investigate the photon energy dependence of photochemical chiral reactions. We formed thin solid films of racemic mixture of alanine on quartz substrates from crystal powders of DL-alanine by using a thermal-crucible vacuum-evaporation system. Sublimation temperature was controlled in the range of 150–200°C and pressure of the vacuum chamber was approximately 5×10^{-2} Pa throughout the evaporation process. The CD spectra of thin solid films just after the deposition were measured from 260 to 160 nm in wavelength using a vacuum-ultraviolet CD beam line BL-12 of HiSOR and confirmed to be mostly zero CD before the irradiation, showing that the spurious CD due to the contamination of film surface were negligible.

The thin solid films of DL-alanine were irradiated with CPL in different wavelengths using the undulator beamline BL1U of UVSOR-III. In case of CPL irradiation in shorter wavelengths than 200 nm, the samples were set in a vacuum sample chamber preventing attenuation by air absorption. On the beam entrance side of the vacuum sample chamber, a gate valve with an MgF₂ vacuum sealing window was mounted. The irradiated CPL wavelengths were 180 and 155 nm corresponding to absorption bands of

alanine molecule. The irradiated photon energy dose was measured with photoelectron current of a silicon photodiode (International Radiation Detectors, Inc.) settled at the sample position.

CD spectra of the CPL irradiated films were measured at BL-12 of HiSOR to clarify the optical activity emergence by CPL irradiation. In order to delete the effects of linear dichroism (LD) and/or linear birefringence (LB) components, the CD spectra were calibrated by measuring the dependence on sample rotation angle (0, 45, 90, and 135 degrees). As the results, the dependence of the CD spectra on the irradiated wavelength and also on the polarization (left- or right-handed) of CPL have been clearly observed (Fig.1) [5,6]. Detailed analysis of CD spectra is in progress to clarify full mechanism of the optical activity emergence, which potentially has relevance to the origin of terrestrial bioorganic homochirality stimulated by CPL.

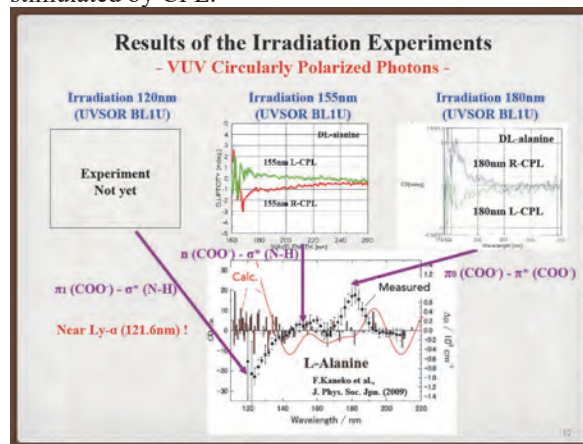


Fig. 1. CD spectra of DL-alanine film after left (L)- or right (R)-handed CPL irradiation.

- [1] W. A. Bonner, *Orig. Life Evol. Biosph.* **21** (1991) 407.
- [2] J. Takahashi *et al.*, *Symmetry* **11** (2019) 919.
- [3] J. Takahashi *et al.*, *Int. J. Mol. Sci.* **10** (2009) 3044.
- [4] F. Kaneko *et al.*, *J. Phys. Soc. Jpn.* **78** (2009) 013001.
- [5] J. Takahashi *et al.*, *UVSOR Activity Report 2018* **46** (2019) 156.
- [6] J. Takahashi *et al.*, *Proc. The 23rd Hiroshima Int. Symp. on Synchrotron Radiation* (2019) 55.

BL1U

Laser Compton Scattering Gamma-ray Generation for Nonlinear Effect in QED

T. Hayakawa^{1,2}, K. Kawase¹, T. Shizuma¹, J. K. Koga³, H. Zen⁴, T. Kii⁴, H. Ohgaki⁴,
M. Fujimoto⁵ and M. Katoh⁵

¹*Tokai Quantum Beam Science Research Center, National Institutes for Quantum and Radiological Science and Applications, Tokai 319-1106, Japan*

²*National Astronomical Observatory of Japan, Mitaka 181-8588, Japan*

³*Kansai Photon Science Institute, National Institutes for Quantum and Radiological Science and Applications, Kizugawa 619-0215, Japan*

⁴*Institute of Advanced Energy, Kyoto University, Uji 611-0011, Japan*

⁵*Institute for Molecular Science, National Institutes of Natural Sciences, Okazaki 444-8585, Japan*

QED predicted unresolved nonlinear effects such as photon-photon interactions. However, because their cross sections are extremely small, the interactions have not been well experimentally measured [1,2]. Delbrück scattering, in which a gamma-ray interacting with a Coulomb field creates an electron-positron pair, which subsequently annihilates to generate a gamma-ray whose energy is almost identical with the incident gamma-ray, is one of important phenomena to study nonlinear effects by QED and vacuum polarization. Koga and Hayakawa [3] have presented that it is possible to measure selectively the amplitude of Delbrück scattering using linearly polarized gamma-ray beams. Furthermore, if one uses a linearly polarized beam with energies lower than 1.022 MeV, which is the threshold of the pair creation, it is possible to measure only the virtual process of Delbrück Scattering, namely vacuum polarization.

For such a purpose, we have developed a laser Compton scattering (LCS) gamma-ray beam with a CO₂ laser having a wavelength of 10.6 μm at the BL1U beamline in UVSOR-III, where the energy of the electron beam stored in top-up mode is approximately 750 MeV. We have demonstrated the 1-MeV LCS gamma-ray beam generation using a randomly polarized CO₂ laser [4].

We newly installed a high power linearly polarized CO₂ laser in order to generate linearly polarized LCS gamma-ray beam. The maximum power of the laser is 130 W. We measured the energy spectra of the generated LCS gamma-ray beam using 3.5" \times 4" LaBr₃(Ce) scintillation detector, and the energy spectra of the photon scattered from a tin or tungsten target with a diameter of 5 mm and a length of 50 mm using two high-purity Ge detectors (see Fig. 1). Figure 2 shows a typical measured energy spectrum. The Compton scattering from the target is clearly observed in the energy region of 400-600 keV. The gamma-ray from natural backgrounds are also observed.



Fig. 1. Photo of the two high-purity Ge detectors at the BL1U beamline.

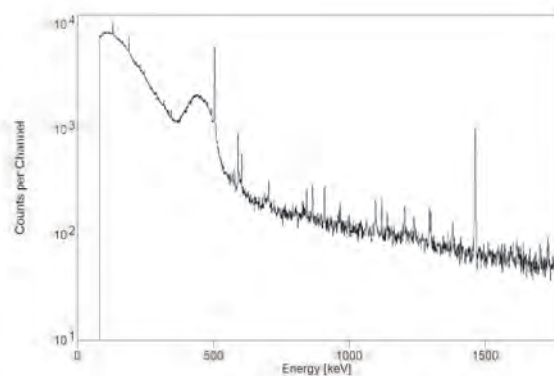


Fig. 2. Typical spectrum of scattered photons from the target, measured by the Ge detector.

[1] ATLAS Collaboration, *Nat. Phys.* **13** (2017) 852.

[2] T. Inada *et al.* *Phys. Lett. B* **732** (2014) 356 .

[3] J. K. Koga and T. Hayakawa, *Phys. Rev. Lett.* **118** (2017) 204801.

[4] H. Zen *et al.*, *J. Phys.: Conf. Ser.* **1067** (2018) 092003.

BL3U

X-ray Absorption Spectra of Lipid Molecules in Bilayer Membranes Measured in Aqueous Solution

R. Tero¹, W.-Z. Goh¹ and M. Nagasaka²¹Toyohashi University of Technology, Toyohashi, 441-8580, Japan²Institute for Molecular Science, Okazaki 444-8585, Japan

The lipid bilayer is a self-assembled structure of amphiphilic lipid molecules, and is the fundamental structure of biomembranes such as cell membranes. Internal structures of lipid bilayers, e.g. two dimensional domains and hydrophobic thickness, and physical properties affect the transportation of materials, information and energy through the biomembranes. All these physiological reactions proceeds in the presence of ions. Ions in the aqueous solution significantly influence to these structures and properties of lipid bilayers. Phosphatidylcholine (PC) (Fig. 1 (a)) is the major component of eukaryotic cells. Cations bind to the phosphate and carbonyl groups of PC. However, affinity of cations to PC, and also other lipids, are still controversy especially in the fields of theoretical simulations [1]. We aim to determine the binding affinity of cations to lipids in aqueous solutions experimentally, by means of X-ray absorption spectroscopy (XAS) [2,3].

We prepared vesicle suspensions of dioleoyl-PC (DOPC) (Fig. 1 (a)), dioctadecenyl-PC (dietherPC) (Fig. 1 (b)), and digalactosyldiacylglycerol (DGDG) (Fig. 1 (c)) in a buffer solution. We introduced the suspension into the XAS flow cell consisting of Si₃N₄ membranes, to form planar lipid bilayers on the Si₃N₄ surface through the process of vesicle fusion method [3]. Fluorescence microscope imaging and fluorescence recovery after photobleaching method showed that DOPC, dietherPC, and DGDG bilayers fully covered the Si₃N₄ membrane surface.

Figure 2 shows O K-edge spectra of the planar lipid bilayers, after subtracted the spectrum of the Si₃N₄ membrane before the lipid bilayer formation. DOPC, which has phosphate and carbonyl groups (Fig. 1 (a)), showed at least two components at 531.06 and 531.94 eV. To identify these components, we measured XAS spectra of dietherPC and DGDG, which have only phosphate group and carbonyl group, respectively (Fig. 2). DietherPC bilayer showed two components at 531.34 and 532.22 eV. We attributed them to 1s→π* transitions of P=O and P-O-Na, respectively, on the basis of inner shell calculation. DGDG bilayer had dominant peak at 532.02 eV. Therefore, the DOPC component at 531.06 eV is attributed to P=O, and that at 531.94 eV to overlapping P-O-Na and C=O.

In conclusion, we obtained XAS spectra of lipid bilayers in an aqueous solution, and identified the components in the spectra. We expect these XAS spectrum components provide information of the effects of cation species and concentration on lipid bilayers.

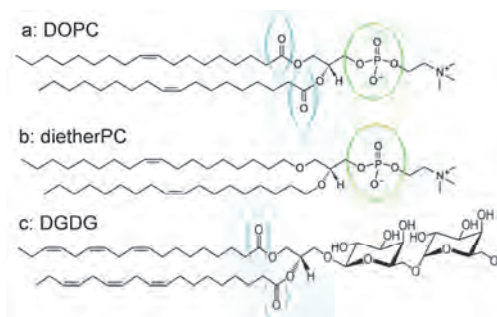


Fig. 1. (a) Dioleoylphosphatidylcholine, (b) dioctadecenylphosphatidylcholine, and (c) digalactosyldiacylglycerol.

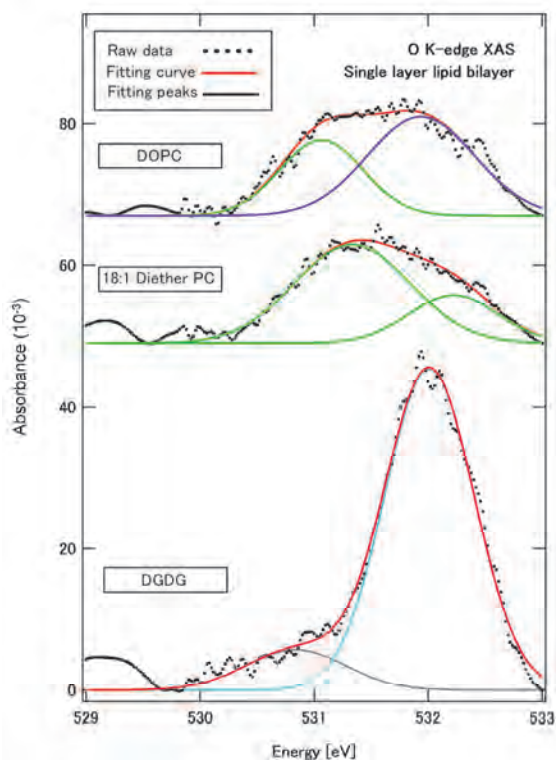


Fig. 2. O K-edge spectra of (a) DOPC, (b) dietherPC, and (c) DGDG bilayers.

- [1] T. B. Woolf, *Biophys. J.* **104** (2013) 746.
 [2] M. Nagasaka, H. Yuzawa, T. Horigome and N. Kosugi, *J. Electron Spectros. Relat. Phenomena* **224** (2018) 93.
 [3] R. Tero, S. Nakamura, Y. Sano and M. Nagasaka, *UVSOR Activity Report* **2018 46** (2019) 158.

BL4U

P-L_{2,3} Absorption Spectra of Phosphates in Plasmid DNA and Adenosine Compounds

T. Ejima¹, T. Ohigashi² and S. Tone³¹IMRAM, Tohoku University, Sendai 980-8577, Japan²UVSOR Synchrotron Facility, Institute for Molecular Science, Okazaki 444-8585, Japan³Sch. of Sci & Technol., Tokyo Denki University, Hatoyama 350-0394, Japan

DNA is composed of simpler monomeric units called nucleotides. The nucleotides are joined to one another in a chain by covalent bonds between the sugar of one nucleotide and the phosphate of the next, resulting in an alternating sugar-phosphate backbone. The phosphate PO₄³⁻ forms ideally a tetrahedral structure in which four oxygen atoms coordinate equidistantly from a center P atom.

The NEXAFS spectrum of the P-K absorption edge in DNA is similar to those of aqueous phosphate (H₂PO₄), biological solids, and animal manures [1,2]. This similarity will be originated from the stable tetrahedral-structure of the phosphate PO₄³⁻. On the other hand, the spectral differences among the phosphate compounds at the P-L_{2,3} absorption edges are remarkable even though the energy positions of the P-L₂ and P-L₃ edges are close to each other [3]. Therefore, it seems natural to focus on P-L_{2,3} absorption edges when shapes and positions of DNA are observed using an X-ray microscope, which is expected to have a high spatial resolution because of the shortness of the observation wavelength [4]. In this study, we focused on the P-L_{2,3} absorption edges (~135 eV) and acquired absorption spectra for the visualization of DNA using the P absorption edges.

Two Adenosine compounds and two DNA were measured: adenosine phosphate (AMP), adenylyl- (5'-3')-adenylyl- (5'-3')-adenosine (AAA), plasmid DNA with a circular structure, and plasmid DNA with a fibrous structure.

The obtained spectra are shown in Figs. 1 and 2. Peak structures are indicated from A to G in the figures and each peak exists at almost the same photon energy positions. The difference among the spectra appears mainly at the peak E.

The density of states of AMP and AAA were calculated to understand the origin of the spectral difference, and the results showed that the P 3d states of AMP and AAA are mainly hybridized with P 3s states and located at around the energy position of peak E. Hence the similarity of the spectral structures between the figures may suggest that the difference of the peak E will be interpreted as the P 3d states difference between the DNAs. Further calculation reflecting the structural difference between the DNAs is necessary for the interpretation of the spectral difference in DNAs.

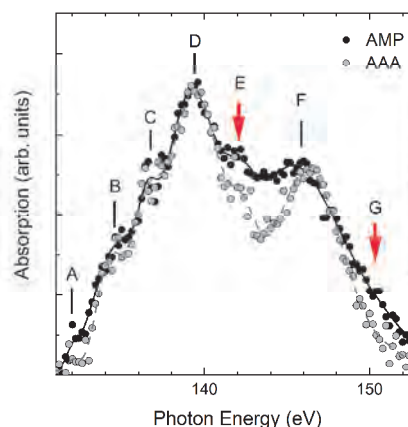


Fig. 1. P-L_{2,3} XAS spectrum of AMP and AAA. Dots represent the measurement results, solid and broken curves are smoothed data.

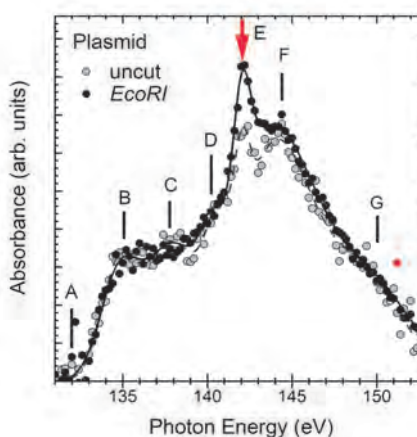


Fig. 2. P-L_{2,3} XAS spectrum of plasmid DNA that air-dried as it is ("uncut"), and that cleaved with EcoRI and air-dried ("EcoRI").

[1] A. Ito, K. Shinohara, Y. Mizukami, H. Nakano, K. Yada, T. Uehara and T. Honda, *J. Synchrotron Rad.* **5** (1998) 1099.

[2] A. L. Shober, D. L. Hesterberg, J. T. Sims and S. Gardner, *J. Environ. Qual.* **35** (2006) 1983.

[3] J. Kruse, P. Leinweber, K.-U. Eckhardt, F. Godlinski, Y. Huc and L. Zuinc, *J. Synchrotron Rad.* **16** (2009) 247.

[4] D. Attwood and A. Sakdinawat, "X-rays and Extreme Ultraviolet Radiation" (Cambridge Univ. Press, 2016, Cambridge, UK) Chap. 11.

[5] W. R. Hunter, "Vacuum Ultraviolet Spectroscopy" (ed. by J. A. Samson and D. L. Ederer, Academic Press, 2000, San Diego, USA) Chap. 11.

BL4U

STXM/XANES Analysis of a Carbonaceous Chondrite Lithology in the Almahata Sitta Meteorite

Y. Kebukawa¹, T. Ohigashi² and M. E. Zolensky³

¹Faculty of Engineering, Yokohama National University, Yokohama 240-8501, Japan

²UVSOR Synchrotron Facility, Institute for Molecular Science, Okazaki 444-8585, Japan

³ARES, NASA Johnson Space Center, Houston, TX 77058, USA

The Almahata Sitta (AhS) meteorite is a brecciated, polymict ureilite that has originated from the near-earth asteroid 2008 TC3 which is classified as an F-type asteroid (a subtype of C complex asteroids) [1]. Carbonaceous chondritic lithologies AhS 671 and AhS 91/91A are known to consist of aqueously altered mineralogy such as phyllosilicates, bruennerite, dolomite, magnetite, fayalite, ilmenite, phosphates, pyrrhotite, and pentlandite, and have similarities to CI1 chondrites, but shows evidence of heterogeneous thermal metamorphism [2]. The textures of AhS 91A and AhS 671 support formation of 2008 TC3 in a regolith environment, and could represent a volume of regolith formed when a carbonaceous chondrite-like body impacted into ureilitic body [2]. Although ureilites usually contain no or little organic matter, it is highly possible that the CI1 lithologies of AhS contain abundant organics as in the case of CI1 chondrites (e.g., Orgueil and Ivuna). To understand the nature of organic matter in CI1 lithologies, and similarity and relationships to primitive carbonaceous chondrites, we analyzed AhS 91A using the scanning transmission X-ray microscope (STXM) at BL4U.

A 100 nm-thick section from AhS 91A was prepared using a focused ion beam equipment at NASA-JSC. C, N, O, Fe-X-ray absorption near-edge structure (XANES) spectra of the sections were obtained using the STXM on BL4U at the UVSOR.

First, we obtained a C-map of the AhS 91A FIB section to locate organic matter. Carbonaceous compounds were distributed partially in the FIB section in sub-micrometer scale (Fig. 1 (a)). Then, “energy stacks” were obtained at C-rich areas. Selected C-XANES spectra generated from the energy stacks are shown in Fig. 1 (b). The C-XANES spectra of the organic-rich regions show large peaks at 284.8 eV due to aromatic carbon, smaller peaks at 286.3 eV and 288.4 eV due to C=O and C(=O)O groups, respectively.

These features are often observed in aqueously altered carbonaceous chondrites (CI, CM, and CR chondrites), with some differences in the intensity ratios of these peaks [e.g., 3]. Some areas are rich in carbonate which is characterized by a large peak at 290.4 eV. There is no $1s\text{-}\sigma^*$ exciton peak at 291.7 eV of graphene structures that is characteristic of thermally metamorphosed chondrites [4]. The molecular structures of organics as well as carbonates, support that the AhS 91A is originated from a aqueously altered carbonaceous chondrite-like parent body [2]. Although some heterogeneous thermal metamorphism are observed in

the AhS 91A, the analyzed region of the AhS 91A has not experienced significant heating events.

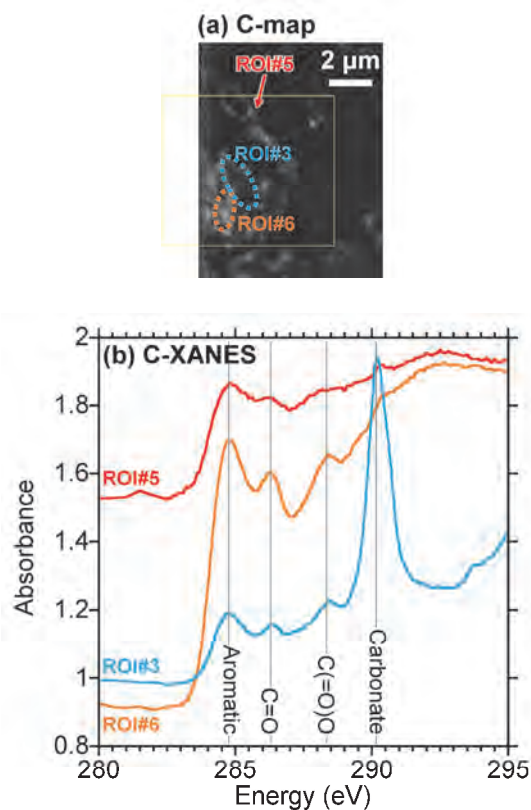


Fig. 1. (a) C-map and (b) C-XANES spectra of the selected regions in the FIB section of AhS 91A.

- [1] P. Jenniskens *et al.*, *Nature* **458** (2009) 485.
 [2] C. A. Goodrich *et al.*, *Meteoritics & Planet. Sci.* **54** (2019) 2769.
 [3] C. Le Guillou *et al.*, *Geochim. Cosmochim. Acta* **131** (2014) 368.
 [4] G. D. Cody *et al.*, *Earth Planet. Sci. Lett.* **272** (2008) 446.

BL4U

Trial of Molecular Mapping for Thin Sections of Isolated Mammalian Nuclei Embedded in Resin Using STXM

A. Ito¹, K. Shinohara², A. Matsuura³, S. Toné⁴, H. Yuzawa⁵ and T. Ohigashi^{5,6}

¹*School of Engineering, Tokai University, Hiratsuka 259-1292, Japan*

²*Graduate School of Health Sciences, Fujita Health University, Toyoake 470-1192, Japan*

³*Research Integrity Office, Fujita Health University, Toyoake 470-1192, Japan*

⁴*School of Science and Engineering, Tokyo Denki University, Hatoyama 350-0394, Japan*

⁵*UVSOR Synchrotron Facility, Institute for Molecular Science, Okazaki 444-8585, Japan*

⁶*School of Physical Sciences, The Graduate University for Advanced Studies, SOKENDAI, Okazaki 444-8585, Japan*

Spectromicroscopy using scanning transmission X-ray microscope (STXM) has been widely accepted as a useful tool to visualize molecular distribution in specimens. Using STXM installed at BL4U of UVSOR, we have been developing an image processing procedure for the quantitative mapping of biomolecules, and successfully applied to the distribution of nucleic acids (DNA and RNA) and proteins such as histone and bovine serum albumin (BSA) in biological specimens using combined NEXAFS at the C, N and O-K absorption edges [1-3]. At present, it is difficult to obtain reliable results for thick specimens such as nucleus area in a whole mammalian cell or an isolated nucleus, due to insufficient transmitted photons through the specimens [3].

Sectioning of a specimen with a thickness as thin as the submicron level is one possible way to cope with such problem. Usually thin sections are made with a microtome for resin embedded specimens. In the present study, we tried to study the thin section of nucleus embedded in organic resin.

Isolated nuclei from human HeLa S3 cells were embedded in Quetol-812 epoxy resin with curing agents, DDSA (dodecyl succinic anhydride) and MNA (methyl nadic anhydride), and a curing promoter DMP-30 (2,4,6-tri(dimethylaminomethyl) phenol) (Nissin EM Co., Ltd., Japan). The section of the resin was made to a thickness of 0.5 μm , and attached on an address mesh (HF-15, Nissin EM) supported with collodion film.

We applied our method to calculate the distributions of nucleic acids and proteins [3] to the observed data for the section specimens. Figure 1 shows the X-ray image of the isolated nucleus at 294 eV (panel a), and composite image of DNA, RNA and histone displayed with different colors (panel b). Contrary to our expectation to be DNA, the main component in the nucleus was found to be RNA. The cause was suspected to be on an analytical process probably due to that the major contribution to the absorbed data was resin.

To improve this situation, we made assumption that images for residual data (spect3) are mainly composed of resin. We generate energy stack file for resin from the spect3 and subtracted it from the original data at the first step of analysis. Our calculation procedure was applied to the thus-obtained stack file. The results are shown in

Figure 2. Three colors, red, green and blue, are given to DNA, RNA and histone for panel a, DNA, RNA and BSA for panel b, and DNA, histone and BSA for panel c, respectively. DNA was found to be the major component in a nucleus, which was in accord with our previous observations for a chromosome [1], and a whole cell [2]. Further analysis is planned to apply to isolated nuclei which undergo apoptosis.

We thank Prof. K. Tohya of Kansai University of Health Sciences for his kind help with making thin sections.

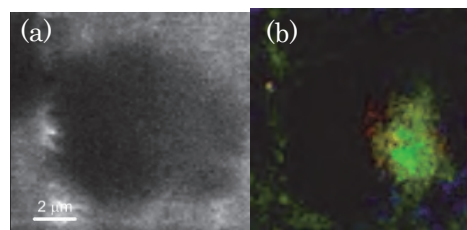


Fig. 1. Isolated nucleus of human HeLa S3 cell. (a) X-ray image at 294 eV, (b) molecular distribution in the nucleus. Red: DNA, Green: RNA, Blue: histone.

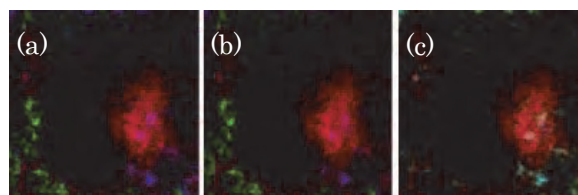


Fig. 2. Improved molecular distribution in the isolated nucleus. (a) DNA (Red), RNA (Green), histone (Blue), (b) DNA (R), RNA (G), BSA (B), (c) DNA (R), histone (G), BSA (B)

[1] K. Shinohara *et al.*, *Ultramicrosc.* **194** (2018) 1.

[2] K. Shinohara *et al.*, *J. X-Ray Sci. Technol.* **26** (2018) 877.

[3] K. Shinohara *et al.*, *Cells* **8** (2019) 8.

BL4U

In situ Analysis for Structure Change of Extraterrestrial Organic Materials During Heating

M. Uesugi¹, M. Ito², K. Tomioka², Y. Kodama³, T. Ohigashi^{4,5}, H. Yuzawa⁴, K. Uesugi¹,
A. Yamaguchi⁶, N. Imae⁶, Y. Karouji⁷, N. Shirai⁸, T. Yada⁹ and M. Abe⁹

¹Japan synchrotron radiation research institute (JASRI/SPring-8), Say-cho 679-5198, Japan

²Kochi Institute for Core Sample Research, Japan Agency for Marine-Earth Science Technology (JAMSTEC),
Nankoku 783-8502, Japan

³Marine Works Japan Ltd., Yokosuka 237-0063, Japan

⁴UVSOR Synchrotron Facility, Institute for Molecular Science, Okazaki 444-8585, Japan

⁵School of Physical Sciences, The Graduate University for Advanced Studies, SOKENDAI, Okazaki 444-8585, Japan

⁶Antarctic Meteorite Research Center, National Institute of Polar Research, Tachikawa 190-8518, Japan

⁷JAXA Space Exploration Center, Japan Aerospace Exploration Agency (JAXA), Sagami-hara 252-5210, Japan

⁸Department of Chemistry, Graduate School of Science, Tokyo Metropolitan University, Hachioji 192-0397, Japan

⁹Institute of Space and Astronautical Science, Japan Aerospace Exploration Agency (JAXA),
Sagami-hara 252-5210, Japan

Organic compounds in extraterrestrial materials are thought to be one of the important components for the building block of the Earth, especially for the origin of life. Those organic materials would be transported to the Earth mostly by micrometeorites, because previous studies suggested that the flux of micrometeorites falling to the Earth is much larger than that of meteorites (5.38×10^4 kg/y for meteorites and 4×10^7 kg/yr for micrometeorites) [1,2]. In addition, micrometeorites show distinct features that their chemical compositions are rather similar to carbonaceous chondrites than any other meteorites [3]. It is well known that most micrometeorites are heated up to 2000 °C during the atmospheric entry, due to atmospheric drag heating. During such intense heating under the oxidized condition, organic compounds would be modified and/or destructed. It is important to evaluate the effect of heating of organic compounds during the atmospheric entry, to investigate origin and evolution of terrestrial organics.

We found that a number of organic nano-globules survived in the Antarctic micrometeorites (AMMs) larger than 150 μm. These AMMs would have experienced intense heating during atmospheric entry due to large moments of inertia, in previous studies [4]. Numerical calculations showed that such AMMs would have heated higher than 1000 °C, and also showed that ram pressure during the heating is almost equivalent to 1 atm.

In order to investigate the possibility of survival of organic matters during heating, we conducted heating experiments of carbonaceous meteorites at 1 atm with 600 °C in atmosphere and 400 °C in N₂ environment, and evaluate the effect on the organic materials using scanning transmission x-ray microscopy and near edge x-ray absorption fine structure (STXM-NEXAFS) analysis. The results of our experiments showed that organic materials were easily destructed and disappeared in oxidized condition, while organics became graphitic and did not disappear during heating in N₂ environment.

The results indicate that organic materials in meteorites would not be destructed by heating in the interplanetary space, because there are less oxygen and water vapor. The organic materials would survive from the heating by irradiation of sunlight, during the transportation from their parent body to the Earth. On the other hand, the organic materials would be easily damaged during the atmospheric entry because of highly oxidized atmosphere.

Survival of organic materials in AMMs suggests that incident velocities of the precursor meteorites are quite low, less around 1 km/s, and/or, their original size is much larger than 1 cm and they would be destructed into smaller pieces during the atmospheric entry. Then unheated materials inside the meteorites can form unheated AMMs.

- [1] Yada T. *et al.*, *Earth Planet Space* **56** (2004) 67.
- [2] Zolensky M. *et al.*, Flux of extraterrestrial materials, in *Meteorites and the early solar system II* (2006) 869.
- [3] Imae N. *et al.*, *Geochim. Cosmochim. Acta* **100** (2013) 116.
- [4] Uesugi *et al.*, Preparation for the analysis of Hayabusa2 returned samples JpGU meeting, abstract (2019).

BL4U

The Behavior of Sulfur in the Past Martian Surface Water Based on STXM-XANES Analysis of Nakhlite Y 000593

H. Suga^{1,2}, K. Suzuki², T. Ohigashi^{3,4}, H. Yuzawa^{3,4}, Y. Takeichi⁵, A. Yamaguchi⁶, T. Usui⁷,
Y. Takahashi² and M. Miyahara⁸

¹Japan Synchrotron Radiation Research Institute (JASRI/SPring-8), Sayo 679-5198, Japan

²The University of Tokyo, Tokyo 113-0033, Japan

³UVSOR Synchrotron Facility, Institute for Molecular Science, Okazaki 444-8585, Japan

⁴The Graduate University for Advanced Studies, SOKENDAI, Okazaki 444-8585, Japan

⁵High-Energy Accelerator Research Organization (KEK), Tsukuba 305-0801, Japan

⁶National Institute of Polar Research, Tachikawa 190-8518, Japan

⁷Japan Aerospace Exploration Agency (JAXA), Sagamihara 252-5210, Japan

⁸Hiroshima University, Higashi-Hiroshima 739-8526, Japan

Nakhlites are intriguing Martian meteorites because they have various secondary minerals formed by water-rock reactions on Mars [1]. The species, assemblages, and chemical compositions of the secondary minerals record the physicochemical properties such as temperature and pH-Eh when the reactions occurred. Hence, the detailed understanding of the secondary minerals allows us to give a new constraint on the physicochemical evolution of the surface water on Mars.

The formation processes of the secondary minerals in nakhlites are enigmatic because carbonate and sulfate minerals coexist in some nakhlites [1-3]: the former precipitates under reductive alkaline condition, the latter under oxidative acidic condition. We examined the sulfide and sulfate minerals in the petrologic thin section of nakhlite Y 000593 (#58-1 stored in NIPR) by FE-SEM-EDS/FE-EPMA at the University of Tokyo, μ -XRF-XAFS at BL-15A of Photon Factory, and STXM-XANES at BL4U of UVSOR to elucidate the formation process of the sulfate minerals.

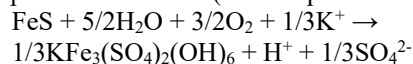
Y 000593 consisted mainly of olivine phenocryst and mesostasis (clinopyroxene, plagioclase, and FeS). Elemental mapping by EPMA showed that a trace amount of sulfur (S) distributed in the carbonate minerals occurring in the fractures of the olivine grains. μ -XRF-XAFS analysis detected the existence of SO_4 in the carbonate minerals. The abundance of S decreased from the rim to the center of the olivine grains. As for the origin of the SO_4 (or sulfate minerals), the only one S-containing mineral in Y 000593 FeS is the candidate.

FE-SEM-EPMA analysis revealed that most of the FeS minerals in the mesostasis of Y 000593 was partly altered. Hence, the oxidation state of the S in the FeS minerals of the mesostasis was measured by μ -XRF-XAFS. The altered portions of the FeS minerals were mainly composed of FeSO_4 .

We tried to clarify the dissolution path of SO_4^{2-} from the FeS minerals to the surrounding minerals (finally, into the fractures of the olivine grains) by FIB-STXM. We made the ultrathin section including the partly

altered FeS minerals by FIB for the STXM analysis. STXM Fe- and S L-edge XANES analysis revealed that the sulfates dissolved from the FeS minerals into the surrounding minerals (Fig. 1).

These results indicate that the origin of SO_4 in the carbonate minerals is the SO_4^{2-} dissolved from the FeS minerals. The chemical reaction formula could be expressed as follows (as a simplified model):



FeS is easily oxidized by liquid water and becomes sulfate mineral jarosite [$\text{KFe}_3(\text{SO}_4)_2(\text{OH})_6$]. Also, this reaction makes sulfate-bearing acid fluid, which decreases the pH. The SO_4^{2-} (and/or jarosite) formed by this reaction should be also the origin of the SO_4 preserved in the carbonate minerals. Carbonate can be easily dissolved by acid fluid. Therefore, we expect that the sulfate minerals in Y 000593 have occurred before the formation of the carbonate minerals as a vein filling precursor.

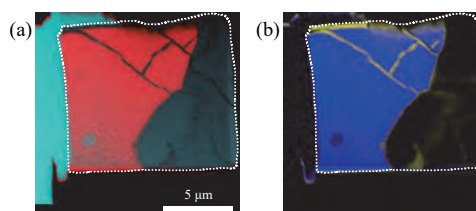


Fig. 1. FIB section scanned by STXM (white dashed line). (a) The red and dark green portions are FeS mineral and plagioclase, respectively. (b) The blue and yellow portions are FeS and FeSO_4 , respectively. Fe^{3+} and SO_4^{2-} dissolved from FeS mineral move into the fractures of plagioclase.

[1] L. M. White *et al.*, *Astrobiology* **14** (2014) 170.

[2] T. Noguchi *et al.*, *JGR* **144** (2009) E10004.

[3] T. Tomkinson *et al.*, *Nat. Commun.* **4** (2013) 2662.

BL4U

Control of Drug Dermal Penetration: Quantitative Probing of Rapamycin

G. Germer¹, T. Ohigashi², H. Yuzawa², R. Flesch¹, F. Rancan³, A. Vogt³ and E. Rühl¹

¹Physical Chemistry, Freie Universität Berlin, Arnimallee 22, 14195 Berlin, Germany

²UVSOR Synchrotron Facility, Institute for Molecular Science, Okazaki 444-8585, Japan

³Charité-Universitätsmedizin, 10117 Berlin, Germany

Progress in quantitative probing of topical drug delivery is reported, which goes beyond our previous work performed at UVSOR III [1,2]. Briefly, hyperspectral imaging of dermal drug penetration is investigated using scanning transmission X-ray microscopy (STXM). The experiments were performed at the BL4U beamline of UVSOR III. They mostly rely on scanning of the photon energy in the O 1s regime (520 – 560 eV), allowing for the acquisition of stacks of images by concentrating on the stratum corneum, the top horny layer of skin. High spatial resolution, corresponding to pixel sizes of 50 nm, allows us to generate in this heterogeneous target reliably reference spectra of the crucial species contained in fixed human skin, especially the topically applied drug rapamycin ($C_{51}H_{79}NO_{13}$, $M=914.13$ g/mol), as well as identification of different skin regions, i.e. corneocytes, lipid layers between the corneocytes, and the fixation medium EPON. Data reduction is performed by using a linear combination of these site-dependently varying contributions, similar to previous work [3]. This yields the local composition of each component. The absolute absorption cross section of the drug is used to determine quantitatively its local concentration and the relation to the dermatologically relevant skin treatment conditions.

Characteristic results are summarized in Fig. 1, which are part of systematic studies. Figure 1 (a) shows the stratum corneum of untreated skin, whereas Fig. 1 (b) shows skin that has been treated for 24 h by 0.1% rapamycin in petroleum jelly. The optical density (OD) recorded at 532 eV is shown in the maps labeled A (top plots in Figs. 1 (a), (b)), clearly indicating the stratified structure of the stratum corneum. The data analysis shown in B clearly distinguishes corneocytes (Cor) (white) from lipids between the corneocytes (Lip) (black), and the viable epidermis (VE) (grey). The maps labeled C show the drug distribution with a clear enhancement, if rapamycin is topically applied (see Fig. 1 (b)). In D the drug concentration is integrated over the maps shown in C as a function of depth, yielding absolute concentrations given in $\text{fmol}/\mu\text{m}^3$, corresponding to a local maximum in drug concentration of ~ 270 $\text{fg}/\mu\text{m}^3$. The reference skin shown in Fig. 1 (a) indicates that no drug is found, but the error bars are sizable due to the data reduction procedure. The sample containing the topically applied drug in petroleum jelly indicates that there are distinct variations in local drug concentration due to the stratified structure of the stratum corneum, where local minima occur in the lipid matrix. This is unexpected for non-polar drugs, such as rapamycin, which are expected to occur primarily in the lipid layers [1]. Clearly, drug penetration is enhanced

by occlusion due to the use of petroleum jelly for formulating the drug. Evidently, this also leads to the uptake of rapamycin into the corneocytes, so that an almost continuous drug distribution is observed in the stratum corneum. There is a characteristic drop in drug concentration near the border to the stratum granulosum, the top layer of the viable epidermis, marked by grey color (see Fig. 1 (b)). This hints that the tight junction barrier is intact so that the drug cannot penetrate efficiently into the viable epidermis.

Systematic studies involving the primary treatment of skin with serine protease for simulating the impact of inflammations have been performed and are currently in preparation for publication [4].

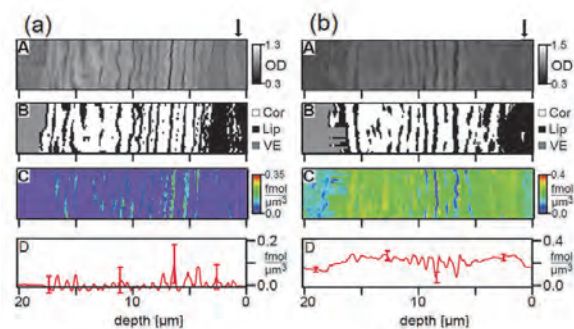


Fig. 1. Results from STXM of the top skin layers of fixed human skin: (a) untreated reference skin and (b) skin treated by rapamycin in petroleum jelly. A: optical density at 532 eV; B: assignment of skin regions due to X-ray absorption characteristics; C: local rapamycin concentration; D: integrated drug concentration as a function of depth. The skin surface is marked by an arrow. See text for further details.

- [1] K. Yamamoto *et al.*, *Anal. Chem.* **87** (2015) 6173.
Eur. J. Pharm. Biopharm. **118** (2017) 30.
Eur. J. Pharm. Biopharm. **139** (2019) 68.
[2] G. Germer *et al.*, UVSOR Activity Report 2018 **46** (2019) 165.
[3] I. N. Koprinarov *et al.*, *J. Phys. Chem B* **106** (2002) 5358.
[4] G. Germer *et al.*, in preparation (2020).

BL4U

Chemical Mapping of Potassium-containing Particles from Residential Biomass Burning and in Ambient Air

X. Kong¹, M. Priestley¹, Z. Wu², T. Ohigashi³, H. Yuzawa³, J. B. C. Pettersson¹
and M. Hallquist¹

¹Department of Chemistry and Molecular Biology, University of Gothenburg, 412 96 Gothenburg, Sweden

²State Key Joint Laboratory of Environmental Simulation and Pollution Control, College of Environmental Sciences and Engineering, Peking University, 100871, China

³UVSOR Synchrotron Facility, Institute for Molecular Science, Okazaki 444-8585, Japan

Burning of wood and other biomass fuels for energy purposes is common on the global scale. Potassium, as one of the main nutrient elements in plants, is released during the burning process and it has been considered as a tracer for biomass burning activities. Here we employed the STXM technique to visualize potassium-containing particles sampled under two circumstances. One is from a campaign at the Research Institutes of Sweden (RISE), where a small-scale wood stove was evaluated regarding its environmental and climate impacts. The other is from field measurements carried out in Beijing with a focus on aerosol properties in the urban environment. The STXM results presented in this study were obtained at the BL4U beamline at UVSOR.

At RISE, aerosol samples were collected from the exhaust line of a wood log burning stove. The major components are soot, organics and inorganic particles. Figure 1 shows the optical density (OD) of a large particle aggregate comprised primarily of a large soot structure with an organic coating that has potassium particles embedded on its surface. Figure 1e shows the difference of OD between the photo energy of (c) 295 eV and (d) 297 eV. The dark spots show the locations where the OD was dramatically enhanced at 297 eV, *i.e.* the potassium L₃-edge. The potassium salt particles seem to attach on the boundaries of the aggregate. Soot is formed in the furnace at high temperatures (> 1000 °C), but under these conditions both organic and potassium compounds are mainly in the gas phase. As temperature is reduced in the exhaust line, potassium compounds first nucleate to form potassium salt particles followed by nucleation and condensation of organics at lower temperatures. The formed potassium-containing particles may agglomerate with existing soot particles, and they are all coated by organics.

Figure 2 shows an OD image of various types of aerosol sampled in Beijing, with a photo energy of 300 eV. Several particles were examined in detail with one example shown here (red square). Full stack scans were performed on this particle at carbon K-edge (potassium L-edge), nitrogen K-edge and sulfur L-edge, respectively. Figures 2 (a)-(c) show the spectra of these three edges on both the core and coating of the particle. Potassium is found in the core region but not on the coatings. The coating mainly contains organic materials. As expected from the chemical complexity of actual atmospheric particles, all of the ammonium, nitrate [1] and sulphate [2] were found in the core of this single particle,

indicating this is a well-aged and -mixed particle with an organic coating.

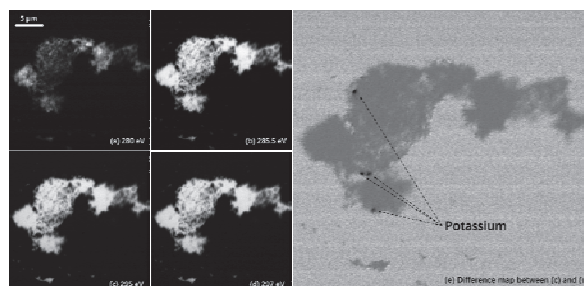


Fig. 1. Optical density of a particle aggregate. The used photo energies are: (a) 280 eV (pre-edge of carbon), (b) 285.5 eV (soot is emphasized), (c) 295 eV (total carbon is emphasized, and also as pre-edge of potassium), and (d) 297 eV (potassium is emphasized). (e) shows the difference between panel (c) and (d).

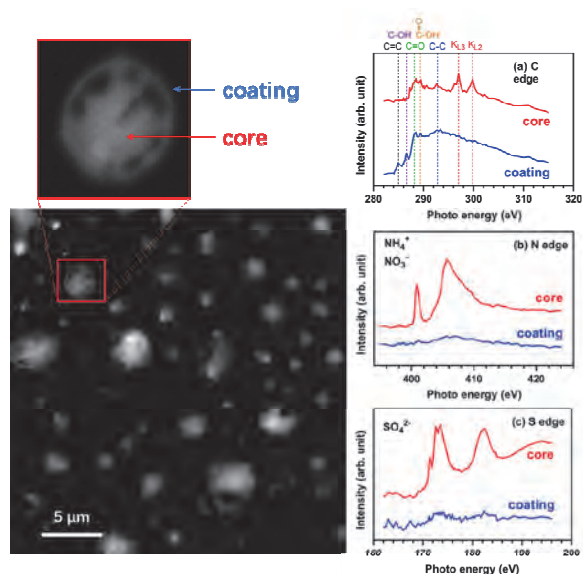


Fig. 2. OD image of urban particles sampled in Beijing. An example particle is scanned at (a) carbon K-edge, (b) nitrogen K-edge and (c) sulfur L-edge, respectively. The spectra measured at the core and on the border were differentiated in red and blue respectively.

[1] Török, S., *et al.*, Powder Diffr. **19** (2004) 81.

[2] Jalilehvand, F., Chem. Soc. Rev. **35** (2006) 1256.

BL4U

Sequestration of Boron in Sediments

Y. Hashimoto¹, K. Kobayashi¹, H. Suga² and Y. Takahashi²

¹*Department of Bioapplications and Systems Engineering, Tokyo University of Agriculture and Technology, Koganei 184-8585, Japan*

²*Department of Earth and Planetary Science, The University of Tokyo, Tokyo 113-0033, Japan*

Boron (B) is ubiquitous in the environment, and major geogenic sources of B in water include desert, saline lake, and spring water. Because short-term and long-term oral exposures to B in animals lead to expressions of reproductive and developmental toxicity [1], the elevated levels of B in water supplies has long been a concern for public health. To lower the environmental risk of B contamination in water, chemical and engineering techniques for removing B from contaminated water have been developed based on physicochemical adsorption, coprecipitation, ion exchange, and reverse osmosis processes. However, the remaining issues for the current techniques in aqueous B removal reside in the inefficiency in cost for materials and reagents (e.g., resin and flocculation chemicals) and B removal capacity and kinetics. Numerous separation materials currently available for aqueous B treatments are less effective for the treatment of water with high levels of B. Therefore, there is an urgent need in the development of cost-effective methods for the treatment of (waste)water with high levels of dissolved B.

The concentrations of B are often high in discharged water from chemical industries and mining and hot spring areas. Boron in the aqueous environment was often found in minerals including calcite and Fe oxide minerals. Knowledge about how B occurs in the environment would help understand the mechanisms of B sequestration and can be used for developing technologies for wastewater with high B concentrations. We examined the distribution of B in sediment collected from a hot spring area with high B conditions using X-ray microscopy (STXM)-based

NEXAFS analyses at UVSOR BL4U. A thin section of sediment was prepared and analyzed for B on the surface.

STXM-based merged B images were obtained at the energy of 188 and 200 eV and their subtraction (Fig. 1). Framboidal pyrite (aspberry-like arrangements of pyrite grains) was found in the sediment and contained B with trigonal and tetrahedral coordination. The distribution of ^{III}B, ^{IV}B and their mixture occupied 4 %, 58 %, and 38 %, respectively. This result indicates that B in this hot spring area occurred mainly with ^{IV}B. Further investigation is needed to reveal the structure of B incorporation to framboidal pyrite.

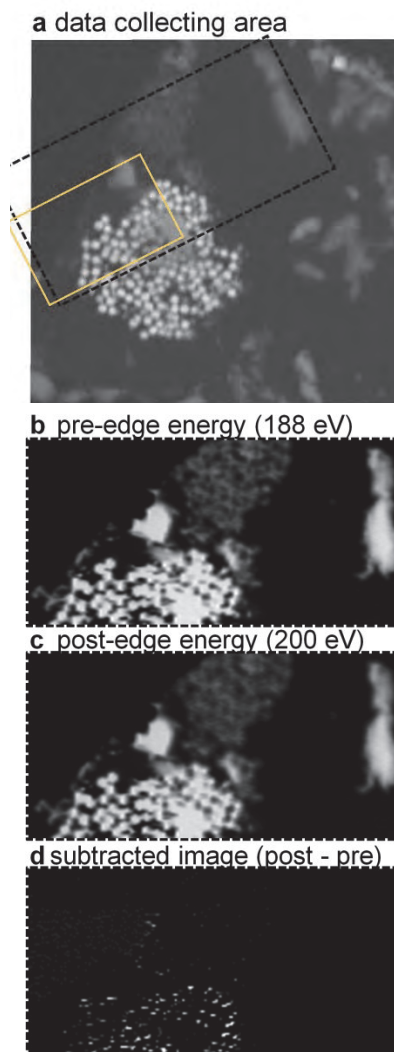


Fig. 1. The SEM image about data collecting area for STXM-based distribution map of boron (a), OD images of pre-edge energy (188 eV, b) and post-edge energy (200 eV, c), and boron distribution map subtracted counts of b from counts of c (d).

[1] WHO (World Health Organization), Guidelines for Drinking-water Quality: First Addendum to the Fourth Edition (2017).

BL4U

Preliminary Results by a STXM-XANES: Analysis of Small Carry-on Impactor Debris Operated by the Hayabusa2 Mission

M. Ito¹, Y. Takano², T. Ohigashi³, H. Yuzawa³, Y. Kebukawa⁴, K. Kiryu⁴, M. Uesugi⁵,
N. Tomioka¹, Y. Kodama⁶, H. Naraoka⁷, T. Yada⁸ and M. Abe⁸

¹Kochi Institute for Core Sample Research, JAMSTEC, Nankoku 783-8502, Japan,

²Biogeochemistry Program, JAMSTEC, Yokosuka 237-0061, Japan,

³UVSOR Synchrotron Facility, Institute for Molecular Science, Okazaki 444-8585, Japan,

⁴Yokohama National University, Yokohama 240-8501, Japan,

⁵JASRI/SPring-8, Sayo-cho 679-5198, Japan,

⁶Marine Works Japan, Yokosuka 237-0063, Japan,

⁷Kyushu University, Fukuoka 819-0395, Japan,

⁸JAXA, Sagami-hara 252-5210, Japan

The JAXA Hayabusa2 mission is a combination of an asteroidal sample return and detailed spectroscopic observations of the C-type asteroid Ryugu for understanding of the Solar System evolution from the point of view of organics, and water as hydrous minerals [1]. The Hayabusa2 spacecraft was thought to be successfully obtained the Ryugu samples (an expected total amount of ~ 100 mg) from surface and subsurface on Feb. and Apr. 2019 and will return to the Earth on Dec. 2020.

To obtain the subsurface samples of the Ryugu, Small Carry-on Impactor (SCI) [2-4] was used to generate an artificial crater on the surface. A force of the SCI was made by HMX (High-Melting Explosive; cyclotetramethylenetetranitramine; C₄H₈N₈O₈, 296.15) together with HTPB (Hydroxyl Terminated Polybutadiene), IDP (Isodecyl palargonate; C₁₉H₃₈O₂) and IPDI (Isophorone diisocyanate; C₁₂H₁₈N₂O₂) [3,4]. Takano and coworkers [5] reported analytical results of SEM-EDS, TD-GC/MS, SPME-GC/MS, and isotope mass spectrometry for N and C isotopes. They found volatiles of aliphatic and aromatic carbon structures, and the several functional groups (hydroxyl, aldehyde, nitrile, and carboxyl) [5].

The explosion products generated by their chemical reactions with HMX, HTPB, IDP and IPDI should be investigated prior to analysis of the Ryugu samples because those materials might be possible contaminants in the subsurface samples in the sample container. In fact, Matsuoka and coworkers pointed out that the low albedo of the asteroid Ryugu could be explained by a combination of C-rich material, grains size, porosity and space weathering effects on the asteroid surface materials [6]. A study of the optical navigation camera on Hayabusa2 space craft reported that the asteroid Ryugu was composed of fluffy cosmic dust particles which is like the carbonaceous materials [7].

It is, therefore, necessary to analyze the SCI fragments and its products for comparison to the Ryugu samples. These results will provide relevant information to the initial analysis in advance the arrival of the Ryugu samples to the Earth.

In this study, we have conducted STXM-XANES

analysis of the experimental explosion-products of the HMX mixture (Fig. 1) for sub-micrometer-scale functional groups of carbon, nitrogen and oxygen. Each fragment shows similar characteristics in O, N but some exceptions of C-XANES in sub-micrometer scale.

To acquire additional chemical properties of the products, we have carried out series of analysis utilizing an optical microscope for micrometer-scale texture, SEM-EDS for texture, microFT-IR for functional groups, micro-Raman for structures of carbonaceous materials. In the future, we will measure hydrogen, carbon and nitrogen isotopes using the JAMSTEC NanoSIMS (nano-scale Secondary Ion Mass Spectroscopy) for further characterizations of the samples.

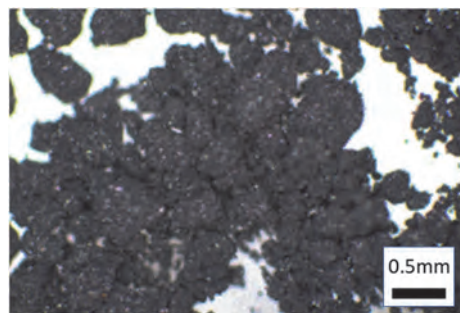


Fig. 1. Experimental products of HMX mixture.

[1] Tachibana *et al.*, *Geochemical Journal* **48** (2014) 571.

[2] Arakawa *et al.*, *Science* **368** (2020) 67.

[3] Saiki *et al.*, *Acta Astronautica* **84** (2013) 227.

[4] Saiki *et al.*, *Space Science Reviews* **208** (2016) 165.

[5] Takano *et al.*, (2014) in *Hayabusa 2014: 2nd Symp. Solar System Materials*, P03.

[6] Matsuoka *et al.* (2019) 50th LPSC (LPI Contrib. No. 2132), abstract#1534.

[7] Okada *et al.*, *Nature* **579** (2020) 518.

BL4U

Characterization of Lysosomal Storage Diseases Using STXM

T. Mansikkala^{1,2}, T. Ohigashi³, H. Yuzawa³, M. Patanen^{1,2}, I. Miinalainen², S. M. Kangas⁴, A. E. Hiltunen⁴, E.-V. Immonen^{1,4}, N. Kosugi³, R. Hinttala⁴, J. Uusimaa⁴ and M. Huttula¹

¹Nano and Molecular Systems Research Unit, PO Box 3000, 90014 University of Oulu, Finland

²Biocenter Oulu, PO Box 5000, 90014 University of Oulu, Finland

³UVSOR Synchrotron Facility, Institute for Molecular Science, Okazaki 444-8585, Japan

⁴PEDEGO Research Unit and Medical Research Center Oulu, and Oulu University Hospital, PO Box 5000, 90014 University of Oulu, Finland

In this work, we have used scanning transmission X-ray microscopy (STXM) technique at BL4U beamline to study patient samples with lysosomal storage diseases and cultured patient-derived fibroblasts with a mutation in NHLRC2 gene. The NHLRC2 encodes an NHL repeat containing protein 2 ubiquitously present in various types of tissues. Mutations in NHLRC2 gene have been linked to fatal cerebropulmonary disease in children with fibrosis, neurodegeneration and cerebral angiomas (FINCA disease), but the functional role of the NHLRC2 is still unknown [1]. Transmission Electron Microscopy (TEM) analysis of immortalized cell cultures from FINCA patients demonstrated multilamellar and multivesicular bodies of unknown cellular origin, and it is suggested that NHLRC2 dysfunction enhances tissue fibrosis [2]. Previously, we reported an STXM study of FINCA patient tissue samples which were in line with TEM results [3].

Our aim was to investigate samples from known lysosomal storage diseases and FINCA disease. Muscle and kidney tissues samples were used, and they had clear enlarged lysosome clusters typical for lysosomal storage diseases. We also had cultured FINCA patient-derived fibroblasts to test if cell culture samples can be imaged. The tissue samples were fixed in 4 % paraformaldehyde and 2.5 % glutaraldehyde in 0.1 M phosphate-buffered saline. Prior to embedding in resin some samples were stained with 1 % OsO₄ and/or uranyl acetate. The 100 nm and 150 nm thick sections of resin-embedded sample were imaged at Biocenter Oulu using a Tecnai G2 Spirit 120 kV TEM (FEI, Eindhoven, The Netherlands) equipped with a Quemesa CCD camera (Olympus Soft Imaging Solutions GmbH, Münster, Germany) to find lysosome clusters on the samples. The same area was then measured with STXM from the subsequent thin sections.

Figure 1 shows example of lysosomes in muscle tissue from patient with a lysosomal storage disease. A cluster analysis of STXM image stacks (Fig. 1 (b)) was performed using a MANTIS software [4]. The cluster analysis was able to differentiate cell components rather consistently based on their spectral information. The spectra obtained at C K-edge are very similar in each cluster as can be seen in Fig. 1 (c). This is caused by the resin that penetrates throughout the tissue and contributes mostly to the spectra. There seems to be no difference between the lysosomes and empty areas filled with resin (blue color in Fig. 1 (b)), indicating that

the material inside lysosomes is lost during the preparation process.

Even though the resin fills the sample, its effect on the spectra can be reduced by removing the resin spectrum from the data. Figure 2 shows an example where the resin spectrum is subtracted with a factor of 0.9 using aXis2000. The exact multiplier is dependent on how much the embedding material penetrates the cell structures and it can vary. By removing the resin, we can detect spectral features that would otherwise be masked by the resin. In Fig. 2 we can see that there is strong peak at 288 eV differing from the typical peak for resin at 288.4 eV. This means that even though it is not ideal, we can study resin embedded samples and provide valuable data from them. However, the goal of identifying the storage material within lysosomes was not achieved.

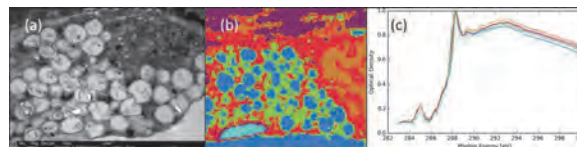


Fig. 1. (a) TEM image of the lysosome cluster from muscle tissue of a patient with lysosomal storage disease. (b) Cluster analysis of lysosomes imaged with STXM from same area as (a) but from a different thin slice. (c) Spectra of the clusters in (b).

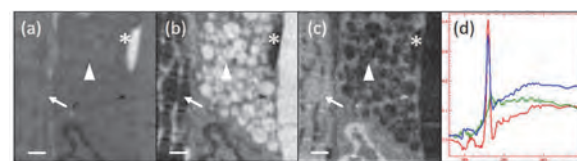


Fig. 2. Locations of fitted spectra in muscle tissue, (a) collagen, (b) lysosomes and (c) muscle fibers. (d) Spectra of the structures, red is collagen (a), green is lysosomes (b) and blue is muscle fibers (c). Collagen fiber bundle is marked with *, lysosomes are marked with Δ and muscle fiber with ↑. Scale bar is 1 μm.

[1] J. Uusimaa *et al.*, *Acta Neuropathol.* **135** (2018) 727.

[2] T. Paakkola *et al.*, *Hum. Mol. Gen.* **27** (2018) 4288.

[3] E.-V. Immonen *et al.*, *UVSOR Activity Report* 2017 **45** (2018) 161.

[4] M. Lerotic *et al.*, *J. Synchr. Rad.* **21** (2014) 1206.

UVSOR User 1

